Model Extended X-ray Absorption Fine Structure (EXAFS) Spectra from Molecular Dynamics Data for Ca2+ and Al3+ Aqueous Solutions

ARTICLE *in* THE JOURNAL OF PHYSICAL CHEMISTRY B · NOVEMBER 2000

Impact Factor: 3.3 · DOI: 10.1021/jp000247i

6 AUTHORS, INCLUDING:

Daniel Spångberg

39 PUBLICATIONS **853** CITATIONS

SEE PROFILE

Kersti Hermansson

Uppsala University

203 PUBLICATIONS **4,688** CITATIONS

SEE PROFILE

Patric Lindqvist-Reis

Karlsruhe Institute of Technology

55 PUBLICATIONS **979** CITATIONS

SEE PROFILE

Farideh Jalilehvand

The University of Calgary

49 PUBLICATIONS **1,119** CITATIONS

SEE PROFILE

Model Extended X-ray Absorption Fine Structure (EXAFS) Spectra from Molecular Dynamics Data for Ca^{2+} and Al^{3+} Aqueous Solutions

Daniel Spångberg and Kersti Hermansson*

Inorganic Chemistry, The Ångström Laboratory, Uppsala University, Box 538, S-751 21, Uppsala, Sweden

Patric Lindqvist-Reis, Farideh Jalilehvand, and Magnus Sandström

Department of Chemistry, Royal Institute of Technology, S-100 44 Stockholm, Sweden

Ingmar Persson

Department of Chemistry, Swedish University of Agricultural Sciences, P.O. Box 7015, S-750 07 Uppsala, Sweden

Received: January 20, 2000; In Final Form: July 18, 2000

Theoretical extended X-ray absorption fine structure (EXAFS) spectra have been computed from molecular dynamics (MD) simulation data. Based on MD-generated molecular geometries, EXAFS spectra were generated with the FEFF6 program, commonly used in the analysis of experimental EXAFS spectra. The effects of multiple scattering and second-shell neighbors on the theoretical spectra were evaluated for $CaCl_2$(aq) and $AlCl_3$(aq), i.e., for two solutions with very different cation hydration structures. The effects are significantly larger for the more structured Al^{3+} solution. The theoretical Ca^{2+}(aq) spectra are compared with new experimental EXAFS data.

1. Introduction

The determination of the solvation structure around metal ions in solution is generally a difficult task. Large-angle X-ray scattering (LAXS) and K- or L-edge extended X-ray absorption fine-structure spectroscopy (EXAFS) are two widely used experimental methods, while on the theoretical side, computer simulations (Monte Carlo, molecular dynamics (MD)) have added valuable and precise molecular-level information concerning both structure and dynamics in aqueous ionic solutions. A comprehensive treatise, which discusses these methods and many others, is given in ref 1, which also summarizes experimental and computational results up to 1993.

Unfortunately, the experimentally determined metal ion−water distances and coordination numbers reported in the literature for one and the same cation often show large deviations. This is not least true for the hydrated Ca^{2+} ion, which is discussed in this paper. Figure 1 shows metal−oxygen distances and coordination numbers from a number of X-ray and neutron diffraction studies.[2−12] In addition to the experimental investigations, there have appeared a number of theoretical simulation studies of Ca^{2+}(aq) in the literature.[10,13−16] Also here the spread of the results is large. The resulting theoretical coordination numbers appear to be higher for the pure ab initio pair potentials (9.0−9.3) than for the potentials where many-body effects have been included, either directly or as an effective pair potential (7.0−8.6). No such systematic conclusions can be made concerning distances, however (2.39−2.54 Å for pure pair potentials and 2.40−2.50 Å for many-body potentials). The star in Figure 1 refers to a recent joint X-ray scattering, EXAFS, and MD study of the hydrated Ca^{2+} ion[12] (here the EXAFS, LAXS, and MD results were consistent).

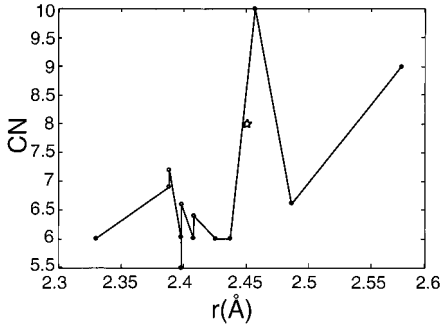

Figure 1. Coordination number plotted against Ca^{2+}−O distances in experimental data from the literature. The star refers to our recent investigation in ref 12. The points are connected to highlight the lack of correlation between distance and coordination number.

We conclude from Figure 1 and from the simulation results for the hydrated Ca^{2+} ion that it is not easy to discern any reasonable trends in the results. One can only hope that the more recent results lie closer to "the truth". The EXAFS method, for example, has steadily developed since synchrotron radiation became more easily available in the 1970s, and the method is now considered a well-developed and mature tool for structural studies (see, for example, ref 17). EXAFS is thus able to yield high-quality information about the local structure around hydrated metal ions, but as always, the generation of high-quality structural quantities requires good facilities and carefully conducted experiments, both during the measurement phase, in the data reduction step, and during the subsequent data analysis. In general, the amplitude error in EXAFS measurements is significantly larger than the phase error, leading to a better determined cation−solvent distance than coordination number. The final data analysis step involves the fitting of the experimental XAFS oscillation, $\chi(k)$, to a model function, which

* Corresponding author. E-mail: kersti.kemi.uu.se.

10.1021/jp000247i CCC: $19.00
Published on Web 10/21/2000

TABLE 1: Number of Molecules in the Different Simulations and Selected Parameters Obtained from the Ca^{2+}−Water Oxygen Radial Distribution Function

					$r_{ion-water}$ (Å)		
potential	n_{waters}	n_{cation}	n_{Cl^-}	concentration (molal)	at first maximum	at first minimum	$n_{ion-water}$ at first minimum
Ca^{2+} (GROMOS)	509	1	2	0.11	2.46	3.31	8.0
Ca^{2+} (Bounds)	509	1	2	0.11	2.51	3.42	9.5
Al^{3+}	200	1	3	0.28	1.96	2.39−3.68	6.0

contains the structural parameters to be derived, such as the distance between the central atom and the backscattering atoms surrounding it, the number of backscatterers in the hydration shell(s), and Debye−Waller parameters describing the thermal width of the distance distribution for each type of distance. The complexity of this fitting function can vary, reflecting the quality of the measured data and the purpose of the study. So, for example, certain parameters, such as the coordination number, can be chosen to be refined or fixed at different trial values. In some cases (although far from always) the fitting model does not consider backscattering from second-shell water molecules. In other cases authors choose not to include multiple scattering in the fitting model, i.e., the raw or Fourier-filtered data are assumed not to contain any contributions from "multilegged" scattering and no angle information is available. Only in the best of cases can the interatomic distances be determined to an accuracy of ±0.01 Å and the coordination number to an accuracy of 10% (see ref 18 and references therein).

As an aid toward a better understanding of the data analysis step, we have here undertaken model calculations to assess the contributions from multiple scattering and from second coordination-shell scattering around two metal ions in aqueous solution: Ca^{2+} and Al^{3+}. The hydration structures around these two ions can be expected to be rather different (and indeed they are, as the radial distribution functions discussed later will show), because the much larger charge-to-radius ratio for the small trivalent aluminum ion compared to Ca^{2+} gives rise to stronger electrostatic interactions between the charged ion and the permanent and induced dipole moments on the surrounding water molecules. The advantage of using *model calculations* to generate the EXAFS spectra for this type of investigation is that we can then pinpoint exactly the feature we are interested in (effect of second shell, effect of multiple scattering, etc.), i.e., one feature at a time, instead of dealing with all the scattering effects at once, as in the case of an experimental spectral analysis. Thus, based on thousands of MD-generated snapshots, theoretical EXAFS spectra were here generated, using the very same computer program[19] as we have previously employed in the analysis of experimental spectra.[12]

Direct modeling of EXAFS spectra from MD simulations and the FEFF program has previously been performed by only a few groups. The method was pioneered by Palmer et al.,[20] who computed EXAFS spectra for Sr^{2+}(aq) with and without hydrogen contributions, using 20 configurations from an MD simulation. Later contributions from the same group have calculated EXAFS spectra for the hydration structure around the Br^- ion[21] and the Ni^{2+} ion.[22] Second-shell and multiple scattering effects were included in those studies. Campbell et al.[23] have compared different contributions to the Fourier transformed EXAFS signal of Cr^{3+}(aq) using thermal parameters obtained from MD simulation.

The layout of the paper is as follows. The MD simulations and the MDFEFF calculations are described in the Method Section together with a brief summary of the data reduction and analysis steps for the experimental reference spectrum. The effects of different contributions to the theoretical spectra, such as the omission of the second hydration shell, the omission of multiple scattering, or the change of coordination figure, were then evaluated. One could add in this connection that, although some previous studies included both second shell and multiple scattering in MD-generated EXAFS data, our way of separating the two effects in a computationally stepwise manner gives some additional clarity to the magnitudes of these two contributions in *k*-space. The results are presented and discussed in the Results section.

2. Method Section

2.1. Calculation of MDFEFF Spectra. *Interatomic Potentials.* The simulations for the $CaCl_2$(aq) and $AlCl_3$(aq) solutions employed very different types of potentials, but this is of no consequence in the present work, because we are only making use of the final MD trajectories and the fact that they represent two systems with very different hydration structures.

In the $CaCl_2$(aq) simulations, the water−water potential used was Jorgensen's potential for pure bulk water, TIP4P.[24] In TIP4P, the site charges are +0.52e at each hydrogen nucleus and −1.04e placed 0.15 Å away from the oxygen toward the hydrogens, and there is also a Lennard-Jones site at the oxygen nucleus. The O−H distance is 0.9572 Å and the H−O−H angle is 104.52°. Two different ion−water Ca^{2+}−H_2O interaction potentials were used, namely that of Bounds[13] and the potential from the GROMOS program.[25] The Cl^-−H_2O potential was taken from Bounds,[13] the Ca^{2+}−Cl^- potential from Probst et al.,[10] and the Cl^-−Cl^- potential from ref 26. No non-Coulombic Ca^{2+}−Ca^{2+} potential was used since it was expected that the distance between the calcium ions would never be short. This was confirmed by inspection of the ion−ion radial distributions.

The $AlCl_3$(aq) potential was taken from ref 27 and incorporates many-body effects. The water−water model used here was a modification of the BJH model.[28] In the BJH model the intermolecular O−O, O−H, and H−H interactions are described by a modified central force model (CF2),[29] augmented with a three-body intramolecular potential for a better description of the intramolecular interactions. The aluminum−water interactions were described by a (2 + 3)-body intermolecular force field in the simulations; namely, a three-body correction was added to the pair-additive energies for all $[Al(H_2O)_2]^{3+}$ triplets where both water molecules reside within 3.5 Å from the Al^{3+} ion. Both the two-body Al^{3+}−water and three-body water−Al^{3+}−water potentials were derived from ab initio calculations and were reported in ref 27. Also, the pair potentials for Cl^-−H_2O, Al^{3+}−Al^{3+}, Al^{3+}−Cl^-, and Cl^-−Cl^- were derived from ab initio calculations.[27]

MD Simulations. Simulations of $CaCl_2$(aq) with the different potential models were performed in the NPT ensemble[30−32] at zero pressure and 300 K (Table 1). Ewald summations were used for the Coulombic interactions.[33] Short-range forces were cut off at 12 Å. The time step used was 0.75 fs. A predictor−corrector integration algorithm was used to obtain the trajectories.[34] Each system was equilibrated for 7.5 ps and the production runs were all 15 ps. A cubic simulation box containing 512 particles (one cation, two anions, and 509 water molecules) was used, giving a concentration of 0.11 *m* (molal).

In the $AlCl_3$(aq) simulation, the basic cube contained 200 water molecules, one cation, and 3 anions representing a 0.28 *m* $AlCl_3$ solution. The Ewald summation technique was used to compute the Coulombic interactions. After equilibration, the simulation was run for 25 ps. The average temperature of the system was close to 300 K, and the total energy was stable to better than 1.0% during the whole run. The resulting $Al^{3+}-O$ distance comes out too long (1.96 Å) compared to experiment[1] (~1.90 Å), but this is of no consequence for the current investigation. Details of the MD simulations can be found in ref 35.

Radial distribution functions were computed from the MD trajectories, according to $g_{cation-O}(r) = n_O(r)/[dV(r)\rho(r)]$, where $n_O(r)$ is the number of oxygen atoms in a small spherical shell at a distance r from the ion, $dV(r)$ is the volume of this shell, and $\rho(r)$ is the number density of oxygen atoms in the whole solution.

Calculation of EXAFS Spectra. EXAFS spectra were calculated with the FEFF program[19] on the basis of molecular positions from the MD snapshots. Temperature-averaged EXAFS spectra were calculated by averaging EXAFS spectra computed from a number of consecutive snapshots. In all cases, only the cation and the oxygen atoms were included in the calculations. The effect of including the second hydration shell, both with and without multiple scattering, was tested.

2.2. Experimental EXAFS Spectra for the $CaCl_2$ Solution. In the following we will make comparisons with an experimental EXAFS spectrum for a 1.5 M $CaCl_2$(aq) solution;[12] in that study the data analysis proceeded as follows. The energy shift, ΔE_0, used in the calibration of the Ca K-edge EXAFS spectra was derived from measurements on a few solids with known structures. The EXAFS oscillations were obtained after standard procedures were performed for pre-edge subtraction, normalization, and spline removal by means of the WinXAS software.[36] Calculated model functions using ab initio-calculated phase and amplitude parameters obtained by the FEFF6 program[19] were curve-fitted to the k^3-weighted data. The asymmetry of the probability distribution of O-atoms in the cation−O shell was modeled with a cumulant expansion of the Debye−Waller factor, including the third cumulant, which compensates for phase shifts in the EXAFS function.[37−38] Fourier transformation was performed over the k-range 3.5−10 $Å^{-1}$ without applying a window function. More details concerning these EXAFS data and the data analysis can be found in ref 12.

3. Results

3.1. $CaCl_2$(aq) Solution. *Comparison of Experimental and Theoretical Spectra.* Figure 2 shows a comparison between the experimental $CaCl_2$(aq) spectrum for the 1.5 M solution and the computed Gromos spectrum for a 0.11 *m* solution. Only the first hydration shell and no multiple-scattering were included in the theoretical spectrum. Simulations performed for concentrations up to 2 *m* gave virtually identical cation−water radial distribution functions, thereby justifying a comparison between simulated and experimental EXAFS spectra. The spectra in Figure 2 are shown for the purpose of ensuring the reader that our calculated spectra are indeed overall very similar to the experimental ones in the interesting k region, and the modifications we will make on our computed EXAFS spectra in the following thus have a direct bearing on the state-of-affairs for experimental spectra.

Effect of Potential, Vibrational Motion, and Coordination Figure on the EXAFS Spectrum. EXAFS model spectra were computed as described in the Method Section. The thermally averaged spectra were all based on 2000 different configurations.

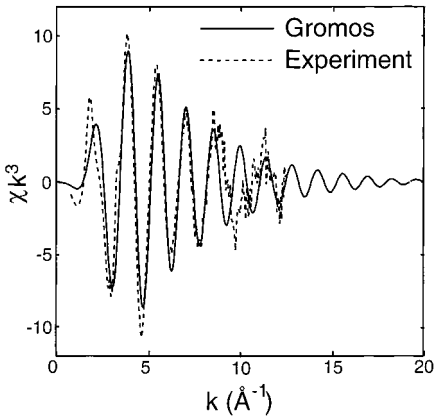

Figure 2. Comparison between experimental (from ref 12) and theoretical EXAFS spectra. For the GROMOS potential the Fermi level was corrected by −1.8 eV. The amplitude of the experimental spectrum was multiplied by 1.964 to obtain the spectrum in the figure.

In the regular FEFF analysis of experimental data, the thermal motion is taken into account by fitting a Debye−Waller factor (or higher cumulants as well) for each type of distance refined. In the MDFEFF analysis, the thermal motion is treated in a more direct way. The vibrational motion of the water molecules and the ions are inherent in the MD simulation method, and the Debye−Waller factors in the subsequent FEFF6 analysis were, of course, set to zero. Figure 3a shows a number of EXAFS spectra computed from a set of MD configurations with the Gromos potential. The three snapshots chosen were arbitrarily taken 7.5 fs apart. As expected, the result is highly dependent on the oxygen−ion distances and destructive interference is seen as a result, when very different distances are present. The Ca−O distance distributions in the three snapshots are given in the figure caption.

Figure 3b shows the result when 2000 such instantaneous EXAFS spectra are averaged. The large instantaneous variation of the geometrical figure (distances and coordination number, but not the angle variation, since no multiple scattering was included) has a very large effect on the individual spectra, but the average effect is smaller. This is further shown in Figure 3c, where the average structures from the Gromos and Bounds simulations are compared.

The GROMOS potentials give rise to a coordination figure, a square antiprism (Figure 4a), which is more or less maintained throughout the simulation. The Bounds potential gives a different coordination number and coordination figure, namely, a tricapped trigonal prism. Sometimes an extra water molecule takes part in the complex, forming a bicapped square antiprism (Figure 4b). Table 1 shows the average Ca^{2+}−water oxygen distances and coordination number for the two different simulations. Both give a fairly well-defined first hydration shell, a distinct second hydration shell (with a maximum at about 4.6 Å), and slight indication of a third hydration shell. The mean coordination number is about 8 with the GROMOS potential and about 9.5 for the Bounds potential. Table 1 shows that, for these two potentials, the average Ca−first shell O distances differ by 0.05 Å; the effect on the final averaged spectra is small but significant.

Effect of the Second Hydration Shell on the EXAFS Spectrum. The experimental spectrum in Figure 2 of course contains contributions from the second hydration shells, while the model used in the data analysis[12] did not. Is this a serious flaw? Figure 5 gives the answer. Two thermally averaged EXAFS spectra from the simulation with the GROMOS potential were computed, one including only the first hydration shell and the other

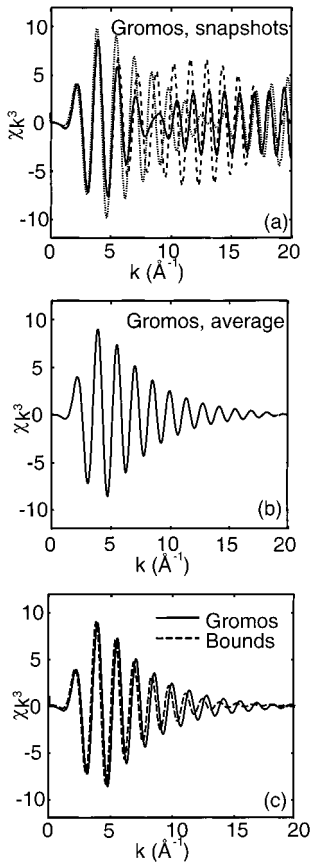

Figure 3. (a) Theoretical EXAFS spectra computed from three different snapshots from the simulation with the GROMOS potential. Here and in panels b and c only the first hydration shell was included in the calculation. The three snapshots have the following Ca−O distance distribution: snapshot 1, four distances of 2.4 Å, two distances of 2.5 Å, and two distances of 2.7 Å; snapshot 2, one distance of 2.3 Å, two distances of 2.4 Å, two distances of 2.5 Å, and three distances of 2.6 Å; and snapshot 3, three distances of 2.4 Å, one distance of 2.5 Å, and four distances of 2.6 Å. (b) Theoretical EXAFS spectrum computed as the average of 2000 snapshots from the simulation with the GROMOS potential. (c) Theoretical EXAFS spectra computed as the average of 2000 snapshots from the simulations with the GROMOS and Bounds potentials.

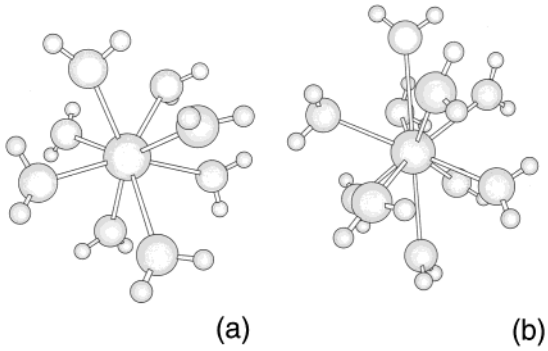

Figure 4. (a) Snapshot from the simulations with the GROMOS potential. (b) Snapshot from the simulation with Bounds potential: a bicapped square antiprism. The removal of the uppermost water gives a tricapped trigonal prism.

including both the first and second hydration shells. The second hydration shell is seen to have an almost negligible effect on the final spectrum. We therefore conclude that the analysis of the experimental data[12] was not seriously affected by the corresponding approximation.

Effect of the Multiple-Scattering Correction of the EXAFS Spectrum. Experimentally, the EXAFS method is not capable

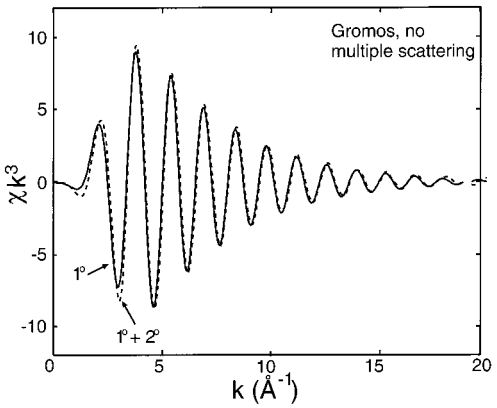

Figure 5. Theoretical EXAFS spectra with the GROMOS potential. One spectrum is for first-shell only; in the other both the first and second hydration shells were included. No multiple scattering was included.

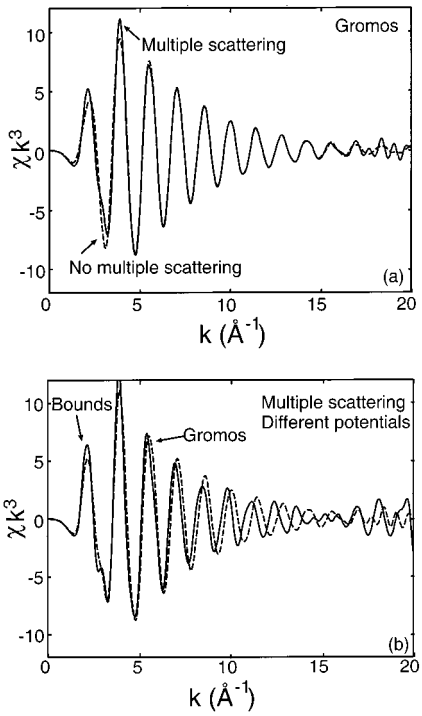

Figure 6. (a) Theoretical EXAFS spectrum with the GROMOS potential and including both the first and second hydration shells. One spectrum includes up to four-legged multiple scattering; the other one has none. (b) Theoretical EXAFS spectrum including both the first and second hydration shells and multiple scattering. One spectrum is from the GROMOS potential simulation, and the other is from the Bounds potential simulation.

of yielding details concerning the coordination geometry, unless multiple scattering makes a significant contribution to the scattering *and* is included in the refinement. Here we will investigate whether multiple scattering makes a large contribution to the EXAFS spectrum in the case of $CaCl_2$(aq).

An EXAFS spectrum was computed including up to four-legged multiple scattering and is compared with the corresponding spectrum without the multiple-scattering correction in Figure 6a. Multiple scattering is seen to give a significant contribution to the spectrum at small k values, although this k range lies outside what is usually included in the fittings of the experimental data. The large discrepancy at large k values is largely an effect of the k^3 scaling in the plot.

Typical snapshots from the two simulations with the GROMOS and Bounds potentials were shown in Figure 4, and thermally averaged EXAFS spectra from the simulations were

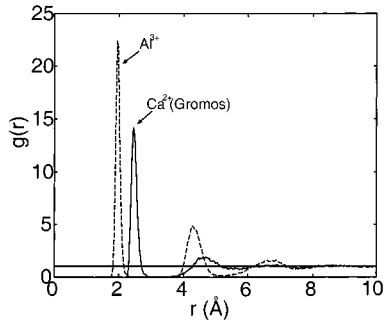

Figure 7. Comparison of the radial distribution functions for Ca^{2+}(aq) and Al^{3+}(aq).

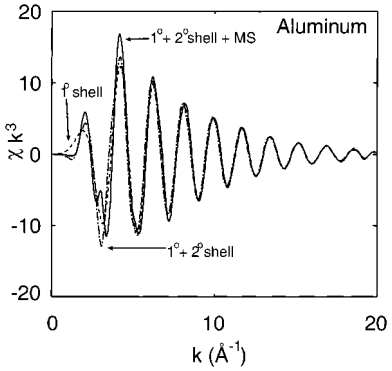

Figure 8. Comparison of theoretical EXAFS spectra of Al^{3+}(aq) including different conditions.

compared in Figure 3c. These spectra did not include any multiple-scattering contributions, and the only spectral feature indicative of a higher coordination number for the Bounds potential is the 0.05 Å longer $Ca^{2+}-O$ distance. Due to this longer distance, the oscillations of the spectrum were shifted to smaller k values. The amplitude also decays faster to zero, indicative of a higher $\langle u^2 \rangle$ value for the water molecules in this simulation. Is it possible to discern more geometrical information if the multiple-scattering contributions are taken into account? Figure 6b shows that the height of the largest peak becomes substantially higher for the geometries resulting from the Bounds potential compared to those from the Gromos potential. The relative heights of the peaks also change. Also, the phase is clearly affected.

3.2. Comparison of $CaCl_2$(aq) and $AlCl_3$(aq) Spectra. Figure 7 shows the radial distribution functions for $CaCl_2$(aq) and $AlCl_3$(aq). The $Al^{3+}-H_2O$ distance is much shorter than the $Ca^{2+}-H_2O$ distance. Note the difference in peak heights between the two solutions, for both the first and the second hydration shells and the deep dip between the second and third hydration shell for Al^{3+} (but not for Ca^{2+}).

Figure 8 shows different theoretical EXAFS spectra for $AlCl_3$(aq) and highlights the second hydration shell and multiple-scattering contributions to the EXAFS spectrum. Similar information for $CaCl_2$(aq) was given in Figure 5 and 6a. Both the amplitude and the phase for $AlCl_3$(aq) are seen to be much more affected by the two contributions than in the calcium solution. Multiple scattering and second-shell backscattering together make a contribution to $\chi(k)$ of approximately 25% in the small-k region for the Al^{3+} solution. This is in large contrast to the hydration structure around Br^-(aq),[21] where the contribution to $\chi(k)$ from the second hydration shell was estimated to be less than 4% and the contribution from multiple scattering was less than 3%. The largest difference between the MD-computed EXAFS spectra for Ca^{2+} and Al^{3+} is caused by the inclusion of the second hydration shell, which is much more ordered for Al^{3+} than for Ca^{2+} (cf. Figure 7).

Concluding Remarks

The MDFEFF-generated EXAFS spectrum for $CaCl_2$(aq) shows an overall good agreement with the experimental spectrum, even when multiple scattering and second-shell contributions are ignored. Each of these contributions has only a small effect on the spectrum (which occurs at small k values). For Al^{3+}(aq) the two contributions have a substantially larger effect on both the spectral oscillations and the amplitude, an effect of the octahedral Al−O coordination and well-defined second shell.

The MD-generated EXAFS spectra are available from the authors on request.

Acknowledgment. We gratefully acknowledge the Swedish Natural Science Research Council and the Foundation for Strategic Research (SSF) for financial support.

References and Notes

(1) Ohtaki, H.; Radnai, T. *Chem. Phys. Rev.* **1993**, *93*, 1157 and references therein.
(2) van Panthaleon van Eck, C. L.; Mendel, H.; Boog, W. *Discuss. Faraday Soc.* **1957**, *24*, 200.
(3) Bol, W.; Gerrits, J. G. A.; van Panthaleon van Eck, C. L. *J. Appl. Crystallogr.* **1970**, *3*, 486.
(4) Licheri, G.; Piccaluga, G.; Pinna, G. *J. Chem. Phys.* **1975**, *63*, 4412.
(5) Licheri, G.; Piccaluga, G.; Pinna, G. *J. Chem. Phys.* **1976**, *64*, 2437.
(6) Caminiti, R.; Licheri, G.; Piccaluga, G.; Pinna, G. *Chem. Phys. Lett.* **1977**, *47*, 275.
(7) Cummings, S.; Enderby, J. E.; Howe, R. A. *J. Phys. C.: Solid State Phys.* **1980**, *13*, 1.
(8) Caminiti, R.; Licheri, G.; Piccaluga, G.; Pinna, G. *Z. Naturforsch.* **1980**, *A35*, 1361.
(9) Hewish, N. A.; Neilson, G. W.; Enderby, J. E. *Nature* **1982**, *297*, 138.
(10) Probst, M. M.; Radnai, T.; Heinzinger, K.; Bopp, P.; Rode, B. M. *J. Phys. Chem.* **1985**, *89*, 753.
(11) Yamaguchi, T.; Hayashi, S.; Ohtaki, H. *Inorg. Chem.* **1989**, *28*, 2434.
(12) Jalilehvand, F.; Spångberg, D.; Lindqvist-Reis, P.; Hermansson, K.; Persson, I.; Sandström, M. *J. Amer. Chem. Soc.*, accepted.
(13) Bounds, D. G. *Mol. Phys.* **1985**, *54*, 1335.
(14) Åqvist, J. *J. Phys. Chem.* **1990**, *94*, 8021.
(15) Floris, F. M.; Persico, M.; Tani, A.; Tomasi, J. *Chem. Phys. Lett.* **1994**, *227*, 126.
(16) Bernal-Uruchurtu, M. I.; Ortega-Blake, I. *J. Chem. Phys.* **1995**, *103* (4), 1588.
(17) *Inorganic Electronic Structure and Spectroscopy*; Solomon, E. I., Lever, A. B. P., Eds.; John Wiley and Sons: New York, 1999.
(18) Jalilehvand, F. *Structure of Hydrated Ions and Cyano Complexes by X-ray Absorption Spectroscopy*; Doctoral Dissertation, Department of Chemistry, Royal Institute of Technology, 2000. http://www.lib.kth.se/Sammanfattningar/jalilehvand000519.pdf.
(19) FEFF6. (a) Zabinsky, S. I.; Rehr, J. J.; Ankudinov, A. L.; Albers, R. C.; Eller, M. J. *Phys. Rev. B* **1995**, *52*, 2995. (b) Ankudinov, A. Ph.D. Thesis, University of Washington, Seattle, WA, 1996. http://leonardo.phys.washington.edu/feff/html/distribution.html.
(20) Palmer, B. J.; Pfund, D. M.; Fulton, J. L. *J. Phys. Chem.* **1996**, *100*, 13393.
(21) Wallen, S. L.; Palmer, B. J.; Pfund, D. M.; Fulton, J. L.; Newville, M.; Ma, Y.; Stern, E. A. *J. Phys. Chem. A* **1997**, *101*, 9632.
(22) Wallen, S. L.; Palmer, B. J.; Fulton, J. L. *J. Chem. Phys.* **1998**, *108*, 4039.
(23) Campbell, L.; Rehr, J. J.; Schenter, G. K.; McCarthy, M. I.; Dixon, D. *J. Synchrotron Radiat.* **1999**, *6*, 310.
(24) Jorgensen, W. L.; Chandrasekhar, J.; Madura, J. D.; Impey, R. W.; Klein, M. L. *J. Chem. Phys.* **1983**, *79*, 926.
(25) van Gunsteren, W. F.; Berendsen, H. J. C. GROningen Molecular Simulation (GROMOS) package, Available from Biomos, n.v. Ninborgh 16, 4767 AG Groningen, The Netherlands, 1987.
(26) Sangster, M. J. L.; Atwood, R. M. *J. Phys. C: Solid State Phys.* **1978**, *11*, 1541.
(27) Bakker, A.; Hermansson, K.; Lindgren, J.; Probst, M. M.; Bopp, Ph. A. *Int. J. Quantum Chem.* **1999**, *75*, 659.
(28) Jancsó, G.; Bopp, P.; Heinzinger, K. *Chem. Phys.* **1984**, *98*, 129.

(29) Stillinger, F. H.;Rahman, A. *J. Chem. Phys.* **1978**, *68* (2), 666.
(30) Andersen, H. C. *J. Chem. Phys.* **1980**, *72*, 2384.
(31) Nosé, S. *Mol. Phys.* **1984**, *52*, 255.
(32) Hoover, W. G. *Phys. Rev.* **1985**, *A31*, 1695.
(33) Ewald, P. *Ann. Phys.* **1921**, *64*, 253.
(34) Gear, C. W. *Numerical initial value problems in ordinary differential equations*; Prentice-Hall: Englewood Cliffs, NJ, 1971.
(35) Bakker, A.; Hermansson, K.; Lindgren, J.; Probst, M. M.; Bopp, Ph. A. *Int. J. Quantum Chem.* (in press).
(36) WinXAS: Ressler, T. *J. Synchrotron Radiat.* **1998**, *5*, 118.
(37) Bunker, G. *Nucl. Instrum. Methods* **1983**, *207*, 437.
(38) Crozier, E. D.; Rehr, J. J.; Ingalls, R. *X-ray Absorption, Principles, Applications, Techniques of EXAFS, SEXAFS and XANES*; Koningsberger, D. C., Prins, R., Eds.; Wiley-Interscience: New York, 1988; Chapter 9.